IEEE Access
Multidisciplinary : Rapid Review : Open Access Journal

Received November 25, 2019, accepted December 8, 2019, date of publication December 18, 2019,
date of current version December 30, 2019.

Digital Object Identifier 10.1109/ACCESS.2019.2960608

Ion-Induced Electrical Isolation in GaN-Based Platform for Applications in Integrated Photonics

KHURRAM HUSSAIN, AHMED SHUJA, MUHAMMAD ALI, ZUBAIR IBRAHIM, AND QAISER MEHMOOD
Center for Advanced Electronics and Photovoltaic Engineering (CAEPE), International Islamic University Islamabad, Islamabad 44000, Pakistan
Corresponding author: Khurram Hussain (khurram.hussain@iiu.edu.pk)

ABSTRACT GaN based Photonic Integrated Circuits (PICs) have now become a global contender for their wide range of applications owing their physical characteristics. The GaN material system acts as a promising platform; compatible with silicon and sapphire substrates. Both the carrier transport and carrier removal techniques are vital to develop the efficient platform for the integration of photonic circuits. We demonstrate the carrier removal mechanism in silicon (Si) doped GaN (0001) epitaxially grown on c-plane sapphire wafer using ion engineering of the devices. Ion-engineered regions within the active layers of the device are modelled, fabricated and characterized to assess the isolation created. Helium and Carbon ions with pre-designed doses and energies are used to irradiate the device structures. We have modelled and fabricated ion-engineered regions within the active layers and studied the carrier transport properties on said regions to isolate that particular part with either of active photonic components placed at the common platform. After ion irradiation, detailed analysis in terms of electric field dependent current characteristics, sheet resistance, carrier mobilities, activation energies, dark and photo currents under zero (ground) and multiple biases are examined to see the extent of charge leakage and to map the charge behavior under nominal operation. Device characteristics under wide regime of annealing temperatures ranging from 300°C to 1000°C are mapped to evaluate the thermal stability of implant driven isolated regions. Activation energies of implanted and parent regions has also been studied. The dark and photon driven electric currents at ground and under biased have been measured to investigate the photo-induced transport phenomenon.

INDEX TERMS Ion implantation, electrical isolation, photonic integrated circuits, crosstalk.

I. INTRODUCTION

GaN with its low thermal generation rates and high breakdown fields promises to be stronger contender for development of future electronic applications, optoelectronic devices [1] and photonic circuits. Besides silicon, the GaN on sapphire (Al_2O_3) substrate is also being considered as a persistent platform for Photonics Integrated Circuits (PICs) [2]. The main advantage of sapphire substrate for GaN devices is its low microwave loss compared to Si based PICs [3]. In recent studies monolithic integration of active and passive components i.e. transmitters, receivers and interconnects are fabricated on the GaN-on-Si platform [4], [5].

In PICs, there may be two or more active (electro-optical) and passive (waveguide) components integrated on a single chip. In order to ensure their efficient operation, there should be no electrical interference between these components for which an electrical isolation region is highly desired. In order to further ensure the planarity of the device surface required for optimum photonic activity, implant isolation is generally preferred over mesa etching. Despite the fact that GaN over silicon has been around for quiet sometime; the Si based platforms are unfavorable to be adopted because of their low optical transmission capability due to their strong visible light absorption. Sapphire, on the other hand can not only minimize the absorption loss but also increase the internal quantum efficiency of overall platform [6], [7] with this pursue; successfully integrated light emitting diodes, photodetectors and waveguides on a single GaN-over-Sapphire platform with minimal optical crosstalk and high data signal rates has recently been achieved [2]. However, one area where potential of GaN-over-sapphire device matrix remains less addressed is to fabricate the well-isolated regions within the PICs to avoid the crosstalk between active and passive components on a pre-designed platform. As multiple photonic components are integrated on a single chip to enhance the

The associate editor coordinating the review of this manuscript and approving it for publication was Jiang Wu.

This work is licensed under a Creative Commons Attribution 4.0 License. For more information, see http://creativecommons.org/licenses/by/4.0/

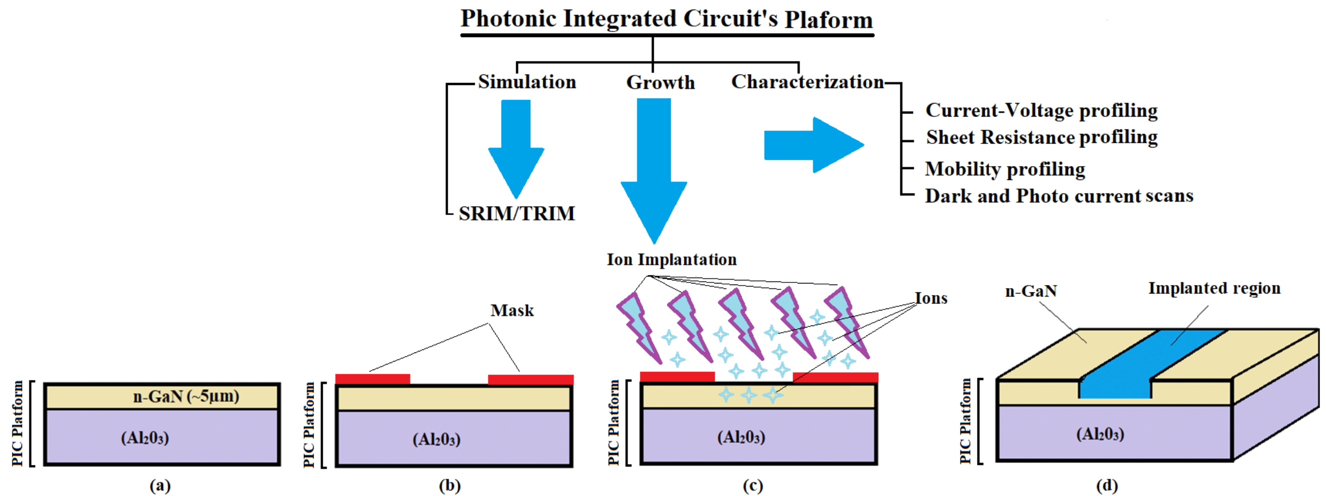

FIGURE 1. **Block diagram and device schematic.**

functionality of a single platform in PICs, it is important to minimize the crosstalk in order to ensure the throughput and integration capacity. This in turn offers advantage like high speed transmission, reduced power consumption, on-wafer testing capabilities and increased system robustness and stability. Ion implantation stands out as an ideal processing tool for doping and implant isolation in III-V semiconductors [8], [9] for versatile applications including the development of PICs [10]. Ion Implantation is known to induce high lattice disorder resulting in decrease of material conductivity and creating highly resistive regions [8]. By selection of appropriate Ion species, their energy and dose of irradiation, and post implant annealing schedules the electrical properties of implanted regions can be tailored and controlled. H^+ [8], He^+ [11], N^+ [12], F^+ [13], Ar^+ [14], Mg^+ [15], Xe^+ [16], O^+ [17], Zn^+ [18], Fe^+ [11] and Kr^+ [19] ions have been employed for implant isolation in GaN or AlGaN devices. Damage-induced mid-gap levels compensation of free carriers in the material and chemically-induced deep levels are generally thought to be two distinct mechanisms of carrier removal to create isolation. We have chosen two species of relatively heavier and lighter ions, namely Carbon (C^+) and (He^+), that may cause inter and intra device isolation within the device matrix for PICs platform. Ion induced engineering of silicon doped GaN over sapphire platform is subsequently undergone a detailed electrical, opto-electronic and carrier transport analysis, to evaluate the potential of the technique for GaN-based PICs development.

In this study we have mapped the detailed analysis on the carrier removal techniques of GaN based photonic ICs. For this we have chosen ion irradiation techniques for inter and intra device isolation within the common photonic platform. To achieve this metrology, we have chosen He^+ and C^+ ions to isolate active region of the photonic platform. To see the extent of this carrier isolation we have initially modelled the ion distribution and its physical damage impact in terms of vacancies created by ion displacements at a particular depth of GaN platform. Physical ion implantations of subject ion are irradiated on GaN platform followed by relatively lower and higher temperature annealing cycles ranging from 300°C to 1000°C. To map the carrier removal phenomena, detailed electrical analysis has been investigated particularly on subject irradiated span of photonic platforms. We have also investigated the photo-induced charge voltaicity on subject areas of GaN device to map its carrier isolation impact at ground (0V) level bias. Also, we have mapped the extent of photo current levels under multiple photonically active bias regimes ranging from 1-5V. Activation energies, sheet resistances and mobilities magnitudes of pre- and post- ion irradiated regions under all subject annealing temperatures have also been investigated in detail.

II. DEVICE SIMULATIONS

Initially the n-GaN matrix shown in Fig. 1 was simulated in Monte Carlo based computer code, namely, Stopping and Ranges of Ions in Matter (SRIM) [20]. The software predicts the ion placement into the device under test with specific dose and ion energy. The ion distribution and vacancy (density profiles) within the device matrix are shown in Fig. 2 for He^+ dose of $1 \times 10^{14} cm^{-2}$ at 800 keV and C^+ dose of $1 \times 10^{14} cm^{-2}$ at multi-energies of 800 keV, 1200 keV and 2500keV; respectively.

The energy schedules were intentionally selected in such a manner to map the damage extent to same depth within the device structure. Normally implant isolation is achieved by employing damage induced deep levels and chemical induced deep levels. For this matter we have employed He^+ ion which would create damage related isolation and for C^+ ion which may also cause mainly the chemical induced isolation. The vacancy and ion distribution profile are another important factor that may critically contribute to the damage related isolation and chemical related isolation respectively within

TABLE 1. Ion-induced isolation schemes.

Dopant Parameter	Implant specie	
	C^+ Ion	He^+ Ion
Ion Energy	- $E_1 = 2500$ keV - $E_2 = 1200$ keV - $E_3 = 800$ keV	- $E_1 = 800$ KeV
Dose	- $D_1 = 1\times 10^{14}$ cm^{-2} - $D_2 = 1\times 10^{14}$ cm^{-2} - $D_3 = 1\times 10^{14}$ cm^{-2}	- $D_1 = 1\times 10^{14}$ cm^{-2}

the device matrix. The average vacancies and ion profiles with respect to the depth into the device for both the cases are presented in Fig. 2. C^+ ion shows greater vacancy profile as compared to He^+ one. This may be due to the heavier mass and physical volume of C^+ ion, however He^+ ion have greater penetration with respect to C^+. The straggles associated with the projected ranges in each case at every implant energy used are within the acceptable limits for our design requirements.

III. EXPERIMENTAL SETUP

To achieve inter and intra device isolation on PICs platform, physical implant schemes are adopted. For this 5 MV pelletron tandem accelerator (5 UDH-2-NEC) was used at National Centre for Physics, Islamabad. Implantation routines are performed on n-type GaN device (Si-doped with $\sim 10^{19}$cm^{-3}) grown on to c-plane both sided polished sapphire's substrate. The initial thickness of n-GaN was about 5μm with Ga-faced polarity. Before ion implantation, samples of size 1cm $\times$ 1cm were cleaved from the parent wafer and cleaned with standard recipe. The multi-implant C^+ and He^+ samples were treated at different devices in each case. The schematic pictorial of overall experimental process and sample's geometry is shown in Fig. 1.

For electrical and electro-optical characterization, I-V metrology system, Hall Effect SWIN-8800 and ASMEC was utilized whereas for post-implant annealing was performed on Rapid Thermal Processor (GSL-1500X-50RTP).

IV. RESULTS AND DISCUSSION

Based on the simulation results, one may predict the closest placement of ions within the device matrix that may be used for the electrical isolation due to the larger extent of physical damage into the device structure. For both the cases larger possibility exists to damage the host and to achieve implant driven carrier isolation phenomena. To gauge the maximum damage into the host lattice we have adopted multi-implant strategy for C^+ (ion) case so that a probable larger number of vacancies are available within the device matrix. For He^+ case, out of the simulated data, a single energy of 800 keV with a dose of 1×10^{14} cm^{-2} was chosen. For both implant cases ion irradiation was performed at a specific region within the device structure with the unwanted area duly capped (refer to Fig. 1) in order to isolate two conductive regions which otherwise are electrically and optically active. The implant parameters for subject isolation schemes are shown in table 1.

This is well established that by ion implantation, surface of host lattice may badly be damaged due to the inter and intra-atomic collisions [21]. As a result, the physical characteristics of device is likely to alter. After the physical ion implantation, the carrier transport properties, the extent of photo currents at different biased voltages and same characteristics at multiple annealing temperatures were investigated to gauge the extent and thermal stability of isolation characteristics. Fig. 3a, 3b & 3c shows the two-point current-voltage characteristics of as implanted, annealed and host n-GaN device matrix.

The He^+ as implant case shows lower current magnitudes as compared to multi implant C^+ cases. This lower current magnitude provides an insight that the extent of damage because of the He^+ ion implantation is more than that of C^+ implants. C^+ being relatively heavier than He atoms may yield larger number of inter and intra-atomic collisions with specific kinetic energies, but its carrier removal rate may get influenced by its relatively higher electro negativity. After ion implantation the said samples was treated under rapid thermal annealing at 500°C for 60 seconds. At this temperature the system contributes less current under given bias due to the possible higher magnitudes of electrical isolation achieved. As the annealing temperature increases further, the carrier removal/isolation capability of the said matrix goes on decreasing. This may be due to chemical nature of carbon atoms as known in some other works for GaN devices [22].

This may also be realized from Fig. 3(a-b) that the applied electric field also influences the current regimes in the device matrix (signature of the extent of damage occurrence within the lattice). For example in Fig. 3(b); for less than one-volt operating voltages (at 0.5 V), the current is in the tune of $\sim 5.75 \times 10^{-11}$ A for samples annealed at 700°C, whereas the similar C^+-implanted samples reflected around 3.65×10^{-9} A when subjected to 1000°C anneals and measured at 0.5V bias. At slightly higher operating voltages, for instance at 5V; the field tends to alter this trend. At 1000°C annealing temperature, C^+ implanted devices show higher extent of leakage, which may be due to carbon atoms acted as chemical impurity with the host of the implant driven lattice damage recovery by virtue of annealing. There may be a possibility of having both of these phenomena occurring at the same time.

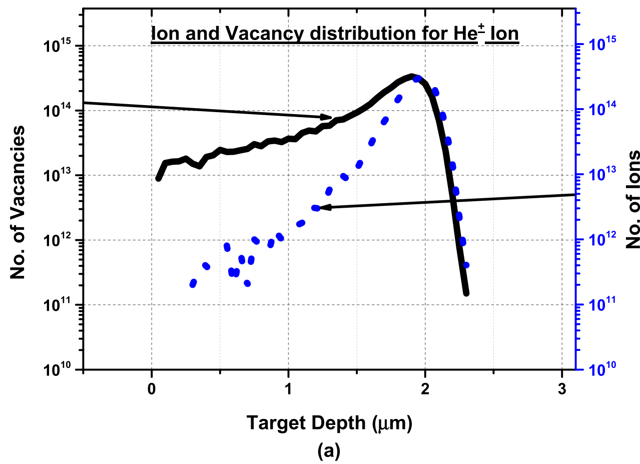

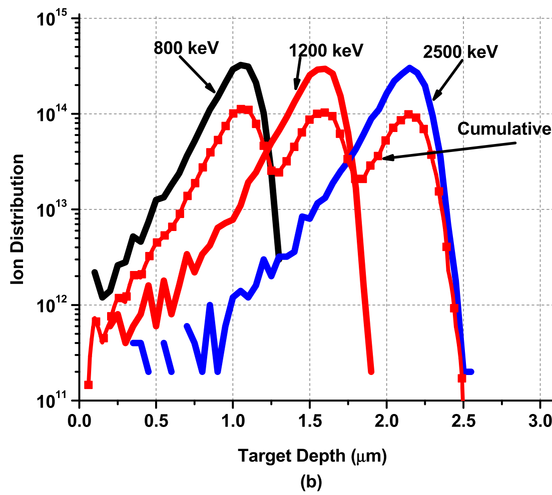

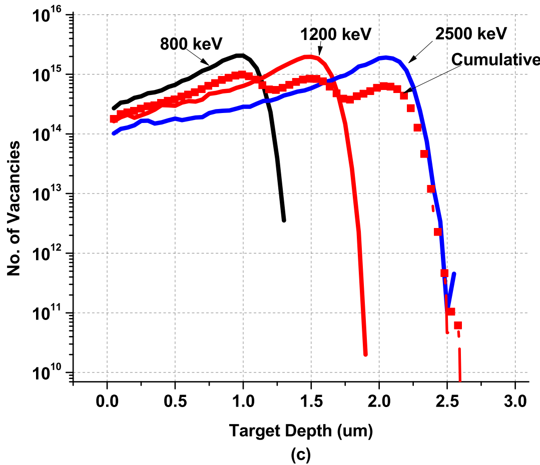

FIGURE 2. Ion distribution and Vacancy profiles (a) He^+ Ion distribution and Vacancy profile, (b) C^+ Ion distribution (c) C^+ Vacancy profile.

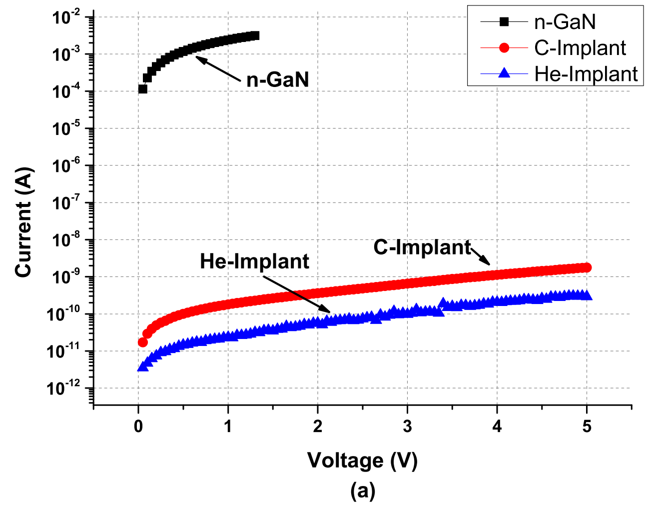

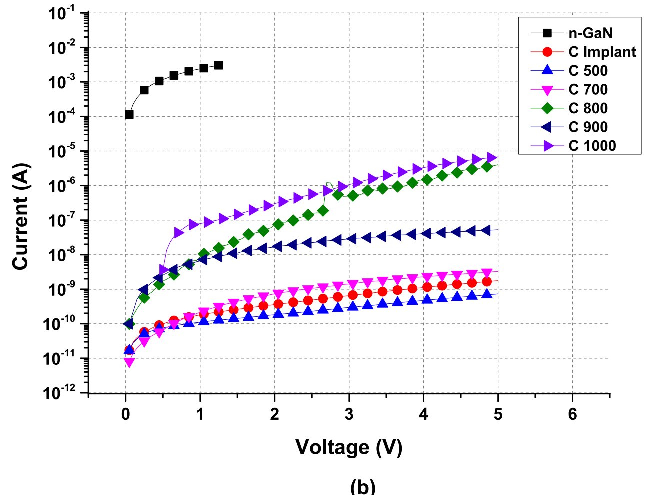

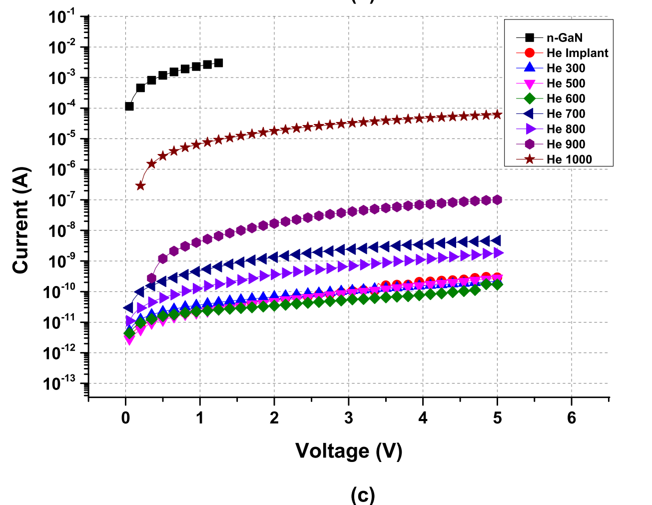

FIGURE 3. Current-voltage characteristics of n-GaN, implant driven electrically isolated regions and post implant annealed devices (a) Comparison of n-GaN, He^+ and C^+ Ion implantation (b) C^+ implantation region, (c) He^+ implantation region.

Fig. 3(c) shows the Current-Voltage (I-V) characteristics of He^+ implanted devices at different annealing temperatures. Likewise, C^+ implant case, He^+ irradiated case shows thermal stability at lower annealing temperatures (300-600°C) and enhances the isolation characteristics. The main advantage of He^+ is its inert nature contributing to the damage alone events. At rather higher annealing temperatures, the charge flow from electrically isolated region tends to increase due to the larger extent of implant driven

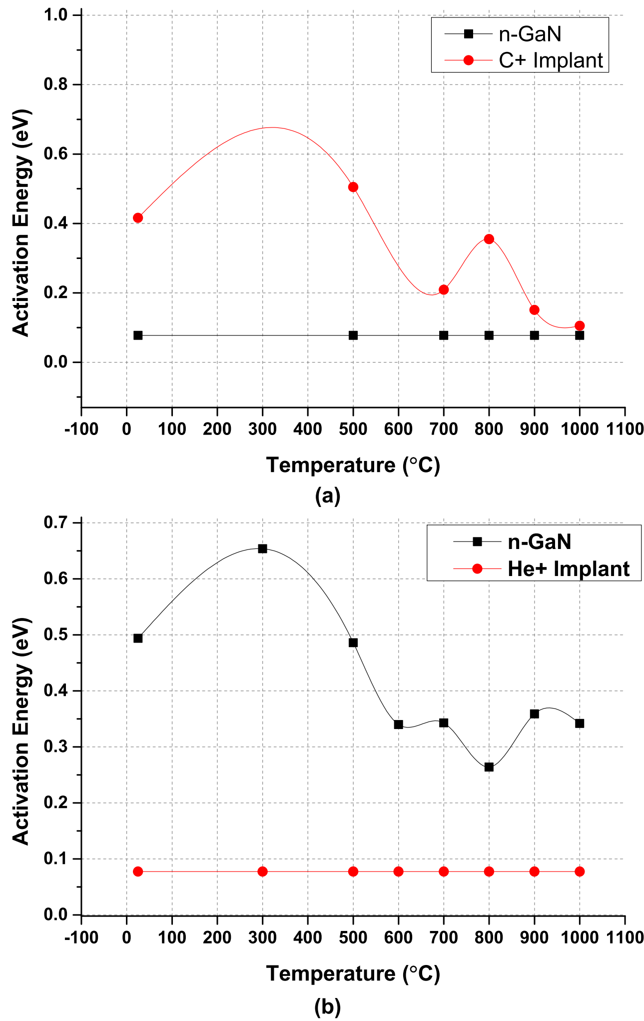

FIGURE 4. Activation Energies of the process (a) C^+ implanted region (b) He^+ implanted region.

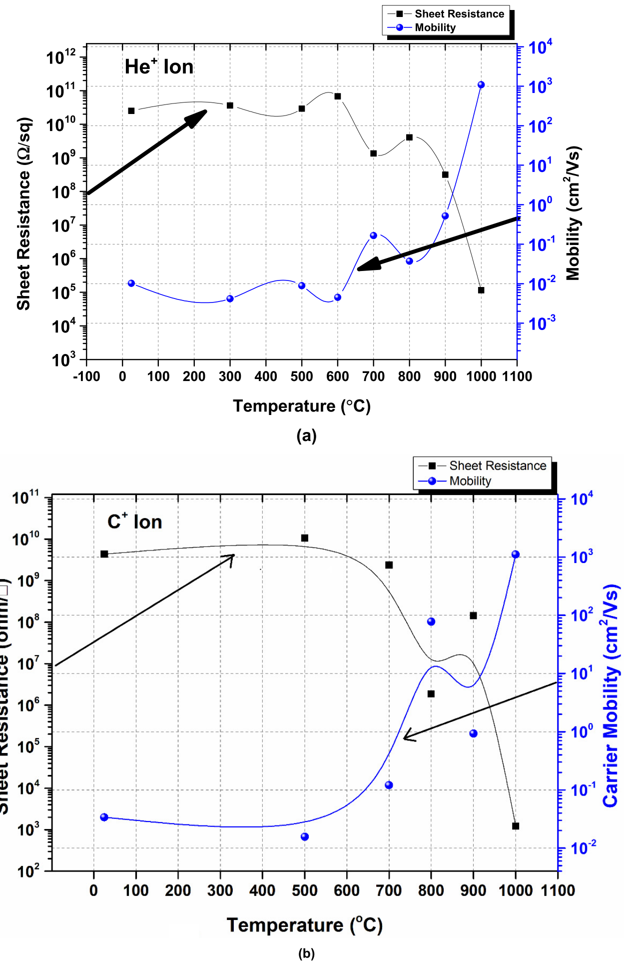

FIGURE 5. Sheet Resistance and Carrier Mobility of implanted GaN matrix at multiple annealing temperatures (a) He^+ Ion irradiation (b) C^+ Ion irradiation.

damage recovery. The charge flow in higher isolation regime approaches 1.7×10^{-10} A at 600°C and the extent of charge leakage increases up to 6.1×10^{-5} A at 1000°C. However, at higher annealing temperatures the trap density rapidly falls below the carrier concentrations and carriers returned to the respective conduction and valence band edges [23]. Although Carbon ion have higher mass than the He^+ ions, but He^+ ion shows ionic size hindrance effect, which is independent of the mass. This limitation explains why Carbon is not able to penetrate deeper into the lattice, even with multiple energy implants [24].

Another parameter that may readily influence the isolation of the inter and intra device regions is the activation energy and governed by the (1) below:

$$\sigma_s = \sigma_o e^{\frac{Ea}{KT}} \tag{1}$$

Here 'σ_s' the conductivity at temperature 'T', 'E_a' is the activation energy, 'K' is the Boltzmann's constant ($= 8.617 \times 10^{-5}$ eVK^{-1}) and 'T' is the temperature in Kelvin. By linear approximation of (1), activation energies for all cases (reference device without implant and annealing; C^+-implanted devices, He^+-implanted devices and post implant annealed devices in both He^+ and C^+ cases) were calculated as shown in Fig. 4(a & b). The activation energy is the minimum energy needed to the carriers (available in the implant driven electrically isolated region) to conduct.

Fig. 4 shows the trend of activation energies for He^+ and C+ implanted devices and those which are annealed after implantation. The activation energy of parent Si doped GaN matrix was around 0.0776 eV, and 0.494 eV and 0.416 eV for an implanted He^+ and C^+ cases; respectively. The higher magnitude of activation energy of He^+ shows that larger physical damage was produced as compared to C^+ implants. Thus, relatively higher energy is needed to conduct He^+ implant region as compared to C^+ isolated region. Consequently, less amount of charge carriers will flow from subject device stack.

For both implant cases the initial thermal flux (300°C for He^+ and 500°C for C^+) enhances the isolation. For effective channel cases for electro-optical and photonic activity, less

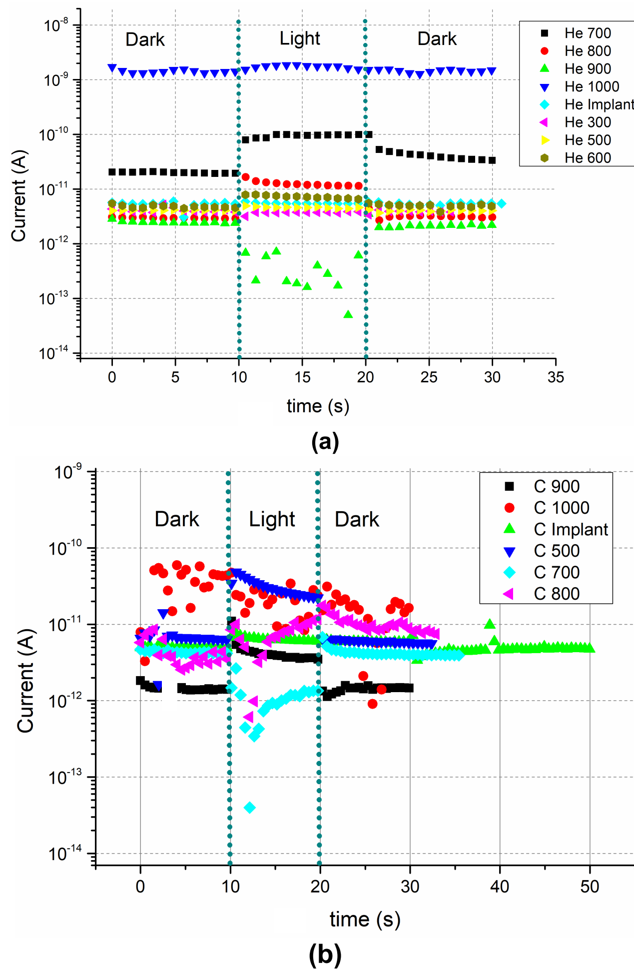

FIGURE 6. Kinetics of dark and luminous current at 0V (a) Kinetics of current of He^+ implant (b) Kinetics of current of C^+ implant.

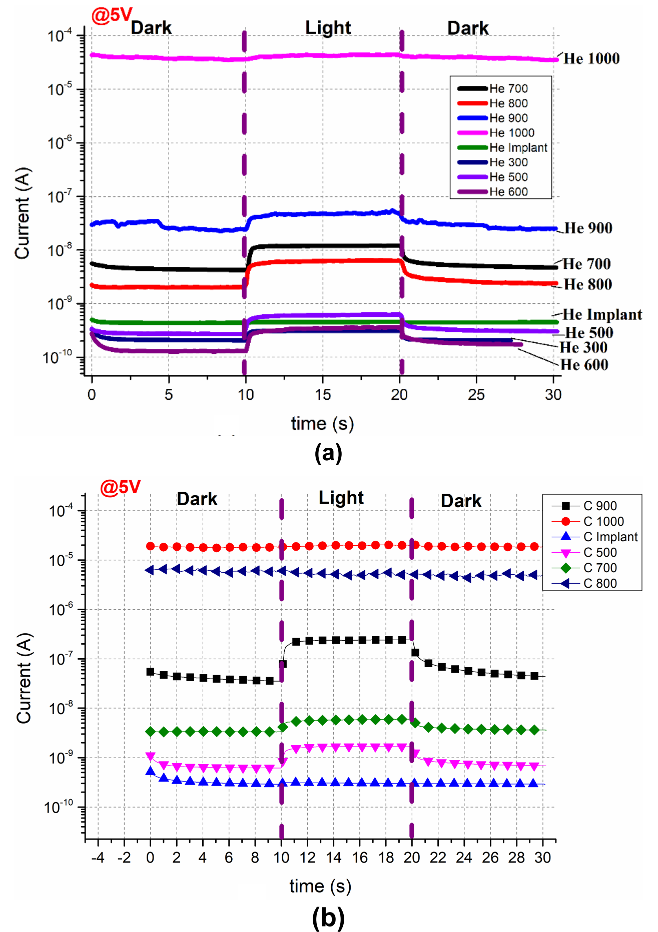

FIGURE 7. Kinetics of dark and luminous current at 5V (a) Kinetics of current in devices with He+ implant (b) Kinetics of current in devices with of C+ implant.

carriers and large amount of activation energy is required so that minimum leakage occurs from subject region. A general rule of thumb for achieving acceptable isolation in GaN device stacks is that the implanted region should have a sheet resistance in the tune of $10^7\,\Omega$/sq [9], [16], [25], [26].

Fig. 5a & 5b shows the sheet resistance and sheet carrier mobility characteristics of all the devices implanted with C^+ and He^+ as well as those which were subsequently annealed. The sheet resistance of initial n-GaN over sapphire platform was measured as 16.9 Ω/sq. When this sample was irradiated with C^+ and He^+ implantation routines (separately), the sheet resistance increases 10^9 times as compared to the parent device. This was primarily thought to be due to defects formed because of the implantation assisted damage of the lattice. As a result of these traps, carriers removed from the bands contributed to significantly increase the sheet resistance [18]. The extent of damage, as shown in Fig. 5, produced from He^+ ion irradiation is larger as compared to C^+ implants.

For all annealed cases, the isolation achieved in the device matrix using He^+ ion is deeper than the multi energy implant C^+ case. Although the carbon multi energy implants produce large extent of physical damage in form of vacancies as compared to He^+ (refer to vacancy profiles in Fig. 2), but the sheet resistivity of He^+ ion cases is relatively higher. This may well be attributed to the chemical nature of Carbon atoms, confirming the results obtained in the I-V analysis of these devices presented in Fig. 3. Carrier mobilities tend to follow the converse trend as compared to the sheet resistance in both the implant cases. The annealing dynamics seen to play a critical role in the recovery of damage in the lattice and consequently improving the conductivity (while reducing the extent of isolation achieved within the GaN-based PIC platform). This behavior is visible in both the device sets in case of He^+ and C^+ implants undergoing a progressively rising annealing temperature cycles.

To inspect the photon driven carrier activation in GaN-based PIC platform, kinetics of electric current under dark and luminous condition at variable electric field was also performed. We have specially employed these measurements at zero applied bias, as well, to inspect the photo-induced charge voltaicity phenomena, for both the implant cases.

TABLE 2. Dark and photo current under different bias conditions for He Ion Implant.

Sample	@0V		@1V		@2V		@3V		@4V		@5V	
	Dark Current (A)	Light Current (A)	Dark Current (A)	Light Current (A)	Dark Current (A)	Light Current (A)	Dark Current (A)	Light Current (A)	Dark Current (A)	Light Current (A)	Dark Current (A)	Light Current (A)
He^{+}-imp	-	-	2.7×10^{-11}	2.8×10^{-11}	6.7×10^{-11}	6.9×10^{-11}	1.3×10^{-10}	1.4×10^{-10}	2.6×10^{-10}	2.7×10^{-10}	4.3×10^{-10}	4.5×10^{-10}
He^{+} 300	3.8×10^{-12}	2.6×10^{-12}	1.6×10^{-12}	2.2×10^{-11}	4.3×10^{-11}	5.8×10^{-11}	8.6×10^{-11}	1.2×10^{-10}	1.4×10^{-10}	2.1×10^{-10}	2.1×10^{-10}	3.1×10^{-10}
He^{+} 500	3.8×10^{-12}	5.0×10^{-12}	1.7×10^{-11}	3.4×10^{-11}	4.1×10^{-11}	8.5×10^{-11}	8.2×10^{-11}	1.9×10^{-10}	1.6×10^{-10}	3.6×10^{-10}	2.7×10^{-10}	6.2×10^{-10}
He^{+} 600	4.4×10^{-12}	8.0×10^{-12}	1.3×10^{-11}	3.0×10^{-11}	1.9×10^{-11}	6.0×10^{-11}	2.3×10^{-11}	1.2×10^{-10}	4.9×10^{-11}	1.9×10^{-10}	1.3×10^{-10}	3.6×10^{-10}
He^{+} 700	1.9×10^{-11}	1.0×10^{-10}	3.6×10^{-10}	6.4×10^{-10}	1.1×10^{-9}	2.5×10^{-9}	2.0×10^{-9}	5.2×10^{-9}	3.1×10^{-9}	8.8×10^{-9}	4.2×10^{-9}	1.2×10^{-8}
He^{+} 800	2.9×10^{-12}	2.5×10^{-11}	1.9×10^{-10}	6.2×10^{-10}	4.8×10^{-10}	1.6×10^{-9}	8.1×10^{-10}	2.7×10^{-9}	1.2×10^{-9}	4.0×10^{-9}	2.0×10^{-9}	6.4×10^{-9}
He^{+} 900	2.4×10^{-12}	1.6×10^{-12}	7.5×10^{-10}	2.0×10^{-9}	4.8×10^{-9}	1.2×10^{-8}	1.1×10^{-8}	2.2×10^{-8}	1.4×10^{-8}	2.9×10^{-8}	2.2×10^{-8}	5.5×10^{-8}
He^{+} 1000	-	-	1.1×10^{-6}	1.6×10^{-6}	3.9×10^{-6}	5.6×10^{-6}	9.4×10^{-6}	1.2×10^{-5}	1.8×10^{-5}	2.3×10^{-5}	3.5×10^{-5}	4.4×10^{-5}

TABLE 3. Dark and photo current under different bias conditions for C Ion Implant.

Sample	@0V		@1V		@2V		@3V		@4V		@5V	
	Dark Current (A)	Light Current (A)	Dark Current (A)	Light Current (A)	Dark Current (A)	Light Current (A)	Dark Current (A)	Light Current (A)	Dark Current (A)	Light Current (A)	Dark Current (A)	Light Current (A)
C^{+}-imp	4.9×10^{-12}	1.0×10^{-11}	8.6×10^{-11}	9.7×10^{-11}	-	-	-	-	-	-	2.9×10^{-10}	3.1×10^{-10}
C^{+} 500	-	-	6.3×10^{-12}	4.9×10^{-11}	4.4×10^{-11}	1.7×10^{-10}	2.3×10^{-10}	5.6×10^{-10}	3.9×10^{-10}	1×10^{-9}	6.2×10^{-10}	1.7×10^{-9}
C^{+} 650	4.2×10^{-12}	-4.8×10^{-12}	1.9×10^{-10}	3.9×10^{-10}	7.3×10^{-10}	1.7×10^{-9}	1.6×10^{-9}	3.6×10^{-9}	2.5×10^{-9}	4.2×10^{-9}	3.3×10^{-9}	6.0×10^{-9}
C^{+} 800	5.6×10^{-12}	1.2×10^{-11}	5.0×10^{-9}	1.4×10^{-8}	2.6×10^{-8}	7×10^{-8}	-	-	-	-	-	-
C^{+} 900	1.4×10^{-12}	1.1×10^{-11}	5.1×10^{-9}	2.5×10^{-8}	1.2×10^{-8}	7.0×10^{-8}	2.1×10^{-8}	1.3×10^{-7}	2.8×10^{-8}	1.9×10^{-7}	3.6×10^{-8}	2.4×10^{-7}
C^{+} 1000	-	-	-	-	-	-	-	-	-	-	-	-

Fig. 6 shows the current kinetics of C^{+} and He^{+} implant driven carrier isolated regions at 0V, for reference point in this study.

During these measurements the samples were subjected initially under dark at a less than 200 lux intensity for 10 seconds and then subjected to luminous conditions at an intensity of about 179000 lux for next 10 seconds followed by another dark condition at 0 volt applied bias. This can be noticed from Fig. 6 that the dark and luminous current have different magnitudes. As these measurements were performed under 0 volts applied bias thus the extent of larger current (during luminous condition) in both cases depicts that the photo-induced potential has developed that is contributing towards the higher magnitude of current. In both the implant cases, for annealing temperature at 1000°C, there is no significant change in current observed.

To gauge the photoconductive phenomena which is essential to address the free carrier loss mechanism in III-nitrides based PICs, we have performed same measurements under different bias conditions i.e. 1V- 5V. The kinetics of current of He^{+} and C^{+} implanted regions at 5V are shown in Fig. 7. This shows that at higher annealing temperature (i.e. 1000 °C) there is no photo response seen i.e. dark and photo currents are same.

This can be noticed from both the as-implant cases that there is hardly any photo response observed. This may be due to the larger extent of physical damage which has prevailed after implantation, confirming the presence of an isolated region. As soon as these implanted samples are treated with thermal flux, they become activated and such physical region can be used as photonic node (transmitter). The exact values of dark and luminous currents under different bias conditions achieved after repetitive measurements are reported in table 2 and table 3 for, He and C ions respectively. These are the magnitudes of dark and photo currents under multiple biased conditions that we have already pointed out spectroscopically in Fig. 6 for 0V and 5V bias regimes under fixed optical power. From these two tables one may clearly see that how much current been increased by incident photons at a particular implanted regions.

V. CONCLUSION

As the free carrier transmission and free carrier loss is an important phenomenon in the efficient development and usage of III-Nitride based PICs; we have studied the ion-induced carrier removal technique in Si-doped GaN on Sapphire platform for integrated photonics applications. The isolation regions were fabricated by the duly simulated multi-energy Carbon and single-energy Helium implantation. The extent of the isolation achieved in both the cases is appreciably over $10^{9}\Omega/\square$. After annealing; owing the progressive damage recovery; the sheet resistance tends to decrease to half or even lesser the value of the optimum isolation achieved in case of Helium and Carbon implant GaN-based PIC platform; respectively. The mobilities of as-implanted and progressively annealed samples signifies the possibility of high and low-free carrier loss during a photonic activity on the integrated platform. Current-voltage (I-V) characteristics of both implant cases provide an insight to possible damage mechanism in relatively "lighter and

inert Helium''- and ''slightly heavier and chemical Carbon''-isolated devices. It is evident from this analysis that for higher annealing temperatures, the conductivity of implanted region increases which eventually contributes to the higher leakage current. Further; the carrier transport/isolation behavior is found dependent on the annealing schedule as well as the applied electric field. The activation energy of non-irradiated device measured as 0.0776eV is found increased manifolds after the combined ion irradiation and annealing cycle at specific temperatures. The dark and photo current investigated especially at ground condition (0V) and at variable bias conditions provided an insight to the photo-conductivities of the ion-induced isolated regions of GaN based PIC platform. Annealing of this device matrix at higher temperatures (such as 1000 °C) yielded no difference in dark and photo currents. The analysis presented in this study may have ramifications for PIC designers for applications in low loss GaN devices under low photon power injection.

REFERENCES

[1] B. J. Baliga, ''Gallium nitride devices for power electronic applications,'' *Semicond. Sci. Technol.*, vol. 28, no. 7, 2013, Art. no. 074011.

[2] K. H. Li, Y. F. Cheung, W. Y. Fu, K. K.-Y. Wong, and H. W. Choi, ''Monolithic integration of GaN-on-sapphire light-emitting diodes, photodetectors, and waveguides,'' *IEEE J. Sel. Topics Quantum Electron.*, vol. 24, no. 6, Nov./Dec. 2018, Art. no. 3801706.

[3] A. W. Bruch, C. Xiong, B. Leung, M. Poot, J. Han, and H. X. Tang, ''Broadband nanophotonic waveguides and resonators based on epitaxial GaN thin films,'' *Appl. Phys. Lett.*, vol. 107, no. 14, 2015, Art. no. 141113.

[4] J. Yuan, X. Gao, Y. Yang, G. Zhu, W. Yuan, H. W. Choi, Z. Zhang, and Y. Wang, ''GaN directional couplers for on-chip optical interconnect,'' *Semicond. Sci. Technol.*, vol. 32, no. 4, 2017, Art. no. 045001.

[5] Y. Jiang, Z. Shi, X. Gao, J. Yuan, S. Zhang, and Y. Wang, ''Monolithic III-nitride photonic circuit for multifunctional visible light communication,'' in *Proc. IEEE/CIC Int. Conf. Commun. China (ICCC Workshops)*, Oct. 2017, pp. 1–2.

[6] H. Y. Ryu, K. S. Jeon, M. G. Kang, H. K. Yuh, Y. H. Choi, and J. S. Lee, ''A comparative study of efficiency droop and internal electric field for InGaN blue lighting-emitting diodes on silicon and sapphire substrates,'' *Sci. Rep.*, vol. 7, 2017, Art. no. 44814.

[7] Y. Cheng, C. Hill, B. Liu, Z. Yu, H. Xuan, D. Homa, A. Wang, and G. Pickrell, ''Modal reduction in single crystal sapphire optical fiber,'' *Opt. Eng.*, vol. 54, no. 10, 2015, Art. no. 107103.

[8] F. T. Johra and W. G. Jung, ''Effect of light-ions implantation on resistivity of GaN thin film,'' *Electron. Mater. Lett.*, vol. 10, no. 4, pp. 699–702, 2014.

[9] D.-S. Kim, J.-H. Lee, S. Yeo, and J.-H. Lee, ''Proton irradiation effects on AlGaN/GaN HEMTs with different isolation methods,'' *IEEE Trans. Nucl. Sci.*, vol. 65, no. 1, pp. 579–582, Jan. 2018.

[10] G. T. Reed, M. M. Milosevic, X. Chen, W. Cao, C. G. Littlejohns, H. Wang, A. Z. Khokhar, and D. J. Thomson, ''Ion implantation in silicon to facilitate testing of photonic circuits,'' *Proc. SPIE*, vol. 10107, Feb. 2017, Art. no. 1010709.

[11] S. Arulkumaran, K. Ranjan, G. I. Ng, J. Kennedy, P. P. Murmu, T. N. Bhat, and S. Tripathy, ''Thermally stable device isolation by inert gas heavy ion implantation in AlGaN/GaN HEMTs on Si,'' *J. Vac. Sci. Technol. B, Nanotechnol. Microelectron., Mater., Process., Meas., Phenom.*, vol. 34, no. 4, 2016, Art. no. 042203.

[12] S. Surender, S. Pradeep, K. Prabakaran, S. S. Menon, I. D. Jacob, S. Singh, and K. Baskar, ''Passivation of yellow luminescence of MOCVD grown InGaN/GaN heterostructures by nitrogen-ion implantation,'' *Nucl. Instrum. Methods Phys. Res. B, Beam Interact. Mater. At.*, vol. 433, pp. 76–79, Oct. 2018.

[13] K. J. Chen, A. M. H. Kwan, and Z. Tang, ''Recent development in flourine-ion-implanted GaN-based heterojunction power devices,'' in *Proc. 1st IEEE Workshop Wide Bandgap Power Devices Appl.*, Oct. 2013, pp. 92–95.

[14] M. Usman, A. Hallén, and A. Nazir, ''Ion implantation induced nitrogen defects in GaN,'' *J. Phys. D, Appl. Phys.*, vol. 48, no. 45, 2015, Art. no. 455107.

[15] T. Narita, T. Kachi, K. Kataoka, and T. Uesugi, ''P-type doping of GaN by magnesium ion implantation,'' *Appl. Phys. Express*, vol. 10, no. 1, 2016, Art. no. 016501.

[16] Y. Li, G. I. Ng, S. Arulkumaran, Z. H. Liu, K. Ranjan, K. S. Ang, P. P. Murmu, and J. Kennedy, ''Improved planar device isolation in AlGaN/GaN HEMTs on Si by ultra-heavy 131Xe+ implantation,'' *Phys. Status Solidi A*, vol. 214, no. 8, 2017, Art. no. 1600794.

[17] M. Grodzicki, P. Mazur, S. Zuber, J. Brona, and A. Ciszewski, ''Oxidation of GaN (0001) by low-energy ion bombardment,'' *Appl. Surf. Sci.*, vol. 304, pp. 20–23, Jun. 2014.

[18] K. Kubota, T. Nishimura, K. Kuriyama, and T. Nakamura, ''Evaluation of lattice displacement and electrical property of Zn-ion implanted GaN by Rutherford backscattering spectrometry,'' *Nucl. Instrum. Methods Phys. Res. B, Beam Interact. Mater. At.*, vol. 451, pp. 70–72, Jul. 2019.

[19] S. Arulkumaran, G. I. Ng, K. Ranjan, G. Z. Saw, P. P. Murmu, and J. Kennedy, ''Improved device isolation in AlGaN/GaN HEMTs on Si by heavy Kr^+ ion implantation,'' in *Proc. 72nd Device Res. Conf.*, Jun. 2014, pp. 115–116.

[20] H. Hofsäss, K. Zhang, and A. Mutzke, ''Simulation of ion beam sputtering with SDTrimSP, TRIDYN and SRIM,'' *Appl. Surf. Sci.*, vol. 310, pp. 134–141, Aug. 2014.

[21] M. Ali, S. Ahmed, F. Younus, and Z. Ali, ''Electrical, charge transients and photo response study of as-deposited and phosphorus implanted Cd1-xZnxTe devices for PV applications,'' *Radiat. Phys. Chem.*, 2019, Art. no. 108498.

[22] S. E. Creutz and J. C. Peters, ''Catalytic reduction of N2 to NH3 by an Fe–N2 complex featuring a C-atom anchor,'' *J. Amer. Chem. Soc.*, vol. 136, no. 3, pp. 1105–1115, 2014.

[23] W. Karl, B. Udo, W. Pohl, W. Karl, B. Udo, and W. Pohl, ''Carrier transport induced and controlled by defects,'' in *Semiconductor Physics*. Cham, Switzerland: Springer, 2018, pp. 1053–1087.

[24] A. A. Kokorina, E. S. Prikhozhdenko, G. B. Sukhorukov, A. V. Sapelkin, and I. Y. Goryacheva, ''Luminescent carbon nanoparticles: Synthesis, methods of investigation, applications,'' *Russian Chem. Rev.*, vol. 86, no. 11, pp. 1157–1171, 2017.

[25] A. Taube, E. Kamińska, M. Kozubal, J. Kaczmarski, W. Wojtasiak, J. Jasiński, M. A. Borysiewicz, M. Ekielski, M. Juchniewicz, J. Grochowski, M. Myśliwiec, E. Dynowska, A. Barcz, P. Prystawko, M. Zajac, R. Kucharski, and A. Piotrowska, ''Ion implantation for isolation of AlGaN/GaN HEMTs using C or Al,'' *Phys. Status Solidi A*, vol. 212, no. 5, pp. 1162–1169, 2015.

[26] J.-Y. Shiu, J.-C. Huang, V. Desmaris, C.-T. Chang, C.-Y. Lu, K. Kumakura, T. Makimoto, H. Zirath, N. Rorsman, and E. Y. Chang, ''Oxygen ion implantation isolation planar process for AlGaN/GaN HEMTs,'' *IEEE Electron Device Lett.*, vol. 28, no. 6, pp. 476–478, Jun. 2007.

KHURRAM HUSSAIN was born in Rawalpindi, Pakistan, in 1977. He received the B.S. degree in electrical engineering from UET, Taxila, in 2001, and the M.S. degree in electrical engineering from NUST, Islamabad, in 2006. He has five years of professional experience in electronics circuit development industry. In 2008, he has joined International Islamic University Islamabad as Assistant Professor. He is actively involved in making research contributions in modern photonics devices and materials for versatile applications.

AHMED SHUJA was born in December 1976. He received the M.S. degree in electrical and electronic engineering from Sweden and the Ph.D. degree in electrical and electronic engineering from U.K. He is currently the Founding Executive Director of the Centre for Advanced Electronics and Photovoltaic Engineering, International Islamic University, Islamabad, Pakistan. Besides serving in EU/U.K., and USA during his professional career, he developed a pioneering teaching and research program, Pakistan, in the area of advanced electronics over a decade ago. His research group studies the engineering of circuits, devices and system for next-generation electronics/optoelectronics, sensing, energy and photonics application-s with cross-disciplinary convergence. He has a track record of publishing rigorously in quality journals, winning numerous funded projects, and actively supervising the research students on diversified problem areas.

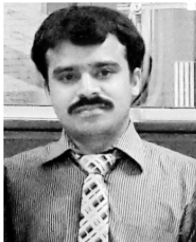

MUHAMMAD ALI was born in Rohillanwali, Muzzafar Garh, Pakistan, in 1993. He received the degree in electronics engineering from Islamia University, Bahawalpur. He joined the Centre for Advanced Electronics and Photovoltaic Engineering (CAEPE), International Islamic University, Islamabad, Pakistan, in 2014. He is actively involved in making research contributions on internationally and nationally funded projects on the forefront of next-generation electronics and photonics devices and materials for versatile applications. He frequently publishes the outcomes of such research in prestigious international journals.

ZUBAIR IBRAHIM was born in Abbottabad, Pakistan, in 1992. He received the B.S. degree in electrical engineering from the Federal Urdu University of Arts, Science, and Technology, in 2015, and the M.S. degree in electrical engineering from International Islamic University, Islamabad, in 2019, where he is currently pursuing the Ph.D. degree.

QAISER MEHMOOD was born in Rawalpindi, Pakistan. He received the B.S. degree in electrical and electronics engineering from the Sarhad University of Science and Information Technology, Peshawar, and the M.S. degree in electrical engineering from International Islamic University Islamabad, Islamabad, in 2019.